

# Characterization of Retinal Microvascular Complications and the Effects of Endoplasmic Reticulum Stress in Mouse Models of Diabetic Atherosclerosis

Vienna Mazzoli,<sup>1</sup> Lexy H. Zhong,<sup>1</sup> Vi T. Dang,<sup>1,2</sup> Yuanyuan Shi,<sup>1</sup> and Geoff H. Werstuck<sup>1-3</sup>

<sup>1</sup>Thrombosis and Atherosclerosis Research Institute, McMaster University, Hamilton, Ontario, Canada

<sup>2</sup>Department of Chemistry and Chemical Biology, McMaster University, Hamilton, Ontario, Canada

<sup>3</sup>Department of Medicine, McMaster University, Hamilton, Ontario, Canada

Correspondence: Geoff H. Werstuck, Thrombosis and Atherosclerosis Research Institute, Hamilton General Hospital Campus, 237 Barton Street E, Hamilton, Ontario, L8L 2X2, Canada;

[geoff.werstuck@taari.ca](mailto:geoff.werstuck@taari.ca)

**Received:** May 8, 2020

**Accepted:** July 27, 2020

**Published:** August 27, 2020

Citation: Mazzoli V, Zhong LH, Dang VT, Shi Y, Werstuck GH.

Characterization of retinal microvascular complications and the effects of endoplasmic reticulum stress in mouse models of diabetic atherosclerosis. *Invest Ophthalmol Vis Sci*. 2020;61(10):49.

<https://doi.org/10.1167/iovs.61.10.49>

**PURPOSE.** Recent evidence suggests that there is a correlation between the micro- and macrovascular complications of diabetes mellitus. The aim of this study is to investigate the molecular mechanisms by which diabetes promotes the development of microvascular disease (diabetic retinopathy [DR]) through characterization of the effects of hyperglycemia in the retina of mouse models of diabetic atherosclerosis.

**METHODS.** Hyperglycemia was induced in apolipoprotein E-deficient (ApoE<sup>-/-</sup>) mice, a model of accelerated atherosclerosis, either through streptozotocin (STZ) injection or introduction of the Ins2<sup>Akita</sup> mutation (ApoE<sup>-/-</sup>Ins2<sup>+Akita</sup>). Another subset of ApoE<sup>-/-</sup> mice was supplemented with glucosamine (GlcN). To attenuate atherosclerosis, subsets of mice from each experimental group were treated with the chemical chaperone, 4-phenylbutyric acid (4PBA). Eyes from 15-week-old mice were either trypsin digested and stained with periodic acid-Schiff (PAS) or frozen for cryostat sectioning and immunostained for endoplasmic reticulum (ER) stress markers, including C/EBP homologous protein (CHOP) and 78-kDa glucose-regulated protein (GRP78). PAS-stained retinal flatmounts were analyzed for microvessel density, acellular capillaries, and pericyte ghosts.

**RESULTS.** Features of DR, including pericyte ghosts and reduced microvessel density, were observed in hyperglycemic and GlcN-supplemented mice. Treatment with 4PBA reduced ER stress in the retinal periphery and attenuated DR in the experimental groups.

**CONCLUSIONS.** Mouse models of diabetic atherosclerosis show characteristic pathologies of DR that correlate with atherosclerosis. The increased magnitude of these changes and responses to 4PBA in the peripheral retina suggest that future studies should be aimed at assessing regional differences in mechanisms of ER stress-related pathways in these mouse models.

**Keywords:** endoplasmic reticulum stress, diabetic retinopathy, retinal microvasculature, hyperglycemia

With the increasing prevalence of diabetes mellitus, microvascular complications of this disease, including diabetic retinopathy (DR), have become a pervasive public health issue worldwide.<sup>1-3</sup> In developed nations, DR is the primary cause of vision loss in the middle-aged population.<sup>4</sup>

In healthy adults, the retinal vasculature remains in a quiescent state, and angiogenic pathways are inactive.<sup>5</sup> Retinal blood vessels provide oxygen and nutrients to inner retinal neurons and facilitate the homeostatic regulation of the retinal environment through the establishment of the inner blood-retinal barrier.<sup>5,6</sup> However, conditions such as diabetes result in extensive vasodegeneration characterized by endothelial cell and pericyte cell loss, capillary dropout, and vascular dysfunction.<sup>7-9</sup> Inflammation and the death of retinal pericytes and endothelial cells compromise the structural integrity and function of retinal blood vessels, resulting in ischemia and, consequently, reductions in visual acuity.<sup>5,10</sup> Since ischemia stimulates

the release of proangiogenic factors leading to vasoproliferation and retinal neovascularization,<sup>5,11,12</sup> hallmarks of DR often include vascular dysfunction, neovascularization, increased vascular permeability, inflammation, and vascular degeneration.<sup>13-16</sup>

The unfolded protein response (UPR) plays a crucial role in maintaining intracellular homeostasis through regulating free calcium storage, as well as the synthesis, folding, and posttranslational modification within the endoplasmic reticulum (ER).<sup>4,15</sup> Diabetes is known to induce ER dysfunction, resulting in the accumulation of misfolded proteins (ER stress) and retinal inflammation.<sup>17-19</sup> In response, cells activate the UPR to enhance protein folding capacity and restore ER homeostasis.<sup>17</sup> In healthy cells, the UPR reduces ER stress levels via upregulation of ER chaperones, promotion of ER-associated degradation of misfolded proteins, and increased regulation of protein translation.<sup>17</sup> However, under conditions of prolonged and irremediable ER stress, the apoptotic

branch of the UPR is activated, causing death of affected cells.<sup>17,20,21</sup>

Although factors such as abnormal glucose and lipid metabolism, oxidative stress, excess cytokine release, and autophagy are likely implicated,<sup>22–24</sup> the pathophysiologic mechanism involved in the progression of DR has yet to be fully elucidated.<sup>25</sup> Interestingly, many of these factors are regulated by pathways involved in the UPR.<sup>25</sup> Studies have shown that sustained hyperglycemia results in oxidative and ER stress, which causes retinal vascular endothelial cell damage and dysfunction as well as retinal neuron death.<sup>23,26–29</sup> Endothelial cell damage can subsequently lead to the destruction of endothelial barrier integrity, causing increased vascular permeability, potentially leading to vision loss.<sup>25,29</sup>

In order to investigate the role of ER stress in the pathogenesis of diabetic complications as well as the links between diabetic micro- and macrovascular disease, we studied DR in three different mouse models of diabetic atherosclerosis.<sup>30–33</sup> Characteristic features of DR were examined in the retinas of mice with increased blood glucose and glucose metabolite levels. The effects of 4-phenylbutyric acid (4PBA), an ER stress inhibitor that attenuates atherosclerosis,<sup>34</sup> were assessed in each of the experimental groups to provide insight into the mechanisms underlying the progression of DR and perhaps an understanding of the links between diabetic micro- and macrovascular disease.

## METHODS

### Animal Models

All experimental and animal handling activities were performed in accordance with the guidelines of institutional Animal Ethics Committee and ARVO Statement for the Use of Animals in Ophthalmic and Vision Research. Mice had unrestricted access to water and standard chow (TD92078; Harlan Teklad, Madison, WI, USA) and were maintained on a 12-hour light/dark cycle throughout the study. All animal procedures were preapproved by, and performed in accordance with, the McMaster University Animal Research Ethics Board and conform to the guidelines of the Canadian Council on Animal Care.

Six-week-old female apolipoprotein E knockout (ApoE<sup>-/-</sup>) mice (B6.129P2-ApoEtm1Unc) were randomly divided into three groups: control, streptozotocin (STZ)-injected, and glucosamine (GlcN)-supplemented groups. Multiple low doses (40 mg/kg/d for 10 days) of STZ (Sigma-Aldrich, St. Louis, MO, USA) were injected intraperitoneally to induce hyperglycemia.<sup>35</sup> GlcN (Sigma-Aldrich) was supplemented in drinking water (5% (w/v)).<sup>36</sup> Female ApoE<sup>-/-</sup> mice were crossed with male ApoE<sup>-/-</sup>:Ins2<sup>+Akita</sup> mice to produce ApoE<sup>-/-</sup>:Ins2<sup>+Akita</sup> offspring.<sup>37</sup> Subsets of control, GlcN-supplemented ApoE<sup>-/-</sup>, STZ-injected ApoE<sup>-/-</sup>, and ApoE<sup>-/-</sup>:Ins2<sup>+Akita</sup> mice were supplemented with 4PBA (1g/kg/d; Scandinavian Formulas Inc., Sellersville, PA, USA) in drinking water. This concentration has been previously shown to attenuate vascular ER stress and atherosclerosis.<sup>34</sup>

### Plasma Analyses

Mice were fasted for 6 hours prior to sacrifice. Fasting blood glucose was measured using an UltraMini blood glucose

meter (OneTouch, Wayne, PA, USA). Mice were then anaesthetized with 3% isoflurane. Blood was collected by cardiac puncture, and mice were euthanized by cervical dislocation. The vasculature was flushed with saline and tissues were collected and prepared for analyses. Fasting plasma insulin was measured by enzyme-linked immunosorbent assay kits (Crystal Chem, Elk Grove Village, IL, USA). Plasma total cholesterol and triglycerides were measured using Infinity reagents (Thermo-Scientific, Waltham, MA, USA).

### Preparation and Staining of the Retinal Vasculature

At 15 weeks of age, all mice were sacrificed and eyes were enucleated. Right eyes were placed in 10% formalin and stored at room temperature. Only left eyes were used for experimental analysis in this study. The left eye was placed in 1× PBS for trypsin digestion or fixation and freezing prior to cryosectioning. Trypsin digestion was performed following the protocol of Chou et al.<sup>38</sup> with minor modifications. Specifically, eyes were pretreated with 70% ethanol for 24 hours prior to incubation in 3% trypsin (Gibco, Waltham, MA, USA) to help increase the efficiency of the digestion process. The trypsin-digested retinas were stained with vascular acid-Schiff (PAS) (Sigma-Aldrich) to visualize the vasculature following the protocol of Dietrich and Hammes.<sup>39</sup>

### Microvessel, Acellular Capillary, and Pericyte Ghost Density Quantification

PAS-stained retinas were imaged at 40× magnification using the automated montage capture function in the Slidebook 5.0 program on an Olympus (Tokyo, Japan) BX41 microscope connected to an Olympus DP72 camera, Prior Scientific Proscan III (Cambridge, UK), and Prior CS152DP joystick. Multiple montages of sections making up the full retina were captured and then compiled using Adobe Photoshop CS6 (Adobe Photosystems, San Jose, CA, USA) to form a single composite image for each retina. A template consisting of 184 sampling boxes aligned along 16 axes with 11 to 12 boxes per axis was centered on the optic disc. The number of microvessels in the first three to four sampling boxes closest to the optic disc was averaged to determine the central retina microvessel density. Likewise, the average number of microvessels in subsequent four sampling boxes corresponded to the microvessel density of the midregion, and that of the final four sampling boxes corresponded to microvessel density of the peripheral region. Retinal microvessel density was estimated using a method similar to that of Browning et al.<sup>40</sup> In this study, the number of vessel intersections within each sampling area was counted for the central, mid-, and peripheral retinal regions.

Acellular capillary and pericyte ghost quantification were based on methods used by Kern and Engerman<sup>9</sup> and Kern et al.<sup>41</sup> Acellular capillaries were defined as having a minimum of one-fourth the width of normal retinal capillaries and lacking nuclei along their length. Acellular capillaries were quantified in the midretinal region. Pericyte ghosts, indicating where pericytes had been lost, were counted as intramural pockets lacking normal cell contents and marked by a faint out-pouching of the capillary basement membrane. Pericyte ghosts were counted only on capillaries containing one or more endothelial cells; otherwise, these capillaries were considered acellular by definition. Pericyte ghosts were

**TABLE.** Metabolic Parameters Measurements From ApoE<sup>-/-</sup> (Control), ApoE<sup>-/-</sup>:Ins2<sup>+Akita</sup> (Akita), GlcN-Supplemented ApoE<sup>-/-</sup> (GlcN), and STZ-Injected ApoE<sup>-/-</sup> (STZ) Groups

Group	4PBA	Glucose (mM)	Insulin (ng/mL)	Triglyceride (mM)	Cholesterol (mM)
ApoE <sup>-/-</sup>	-	8.3 ± 0.14	0.49 ± 0.17	1.2 ± 0.4	7.6 ± 1.5
	+	8.6 ± 0.8	0.44 ± 0.17	1.0 ± 0.5	7.7 ± 1.4
GlcN	-	8.7 ± 0.9	0.52 ± 0.1	1.1 ± 0.3	8.0 ± 1.6
	+	8.3 ± 0.9	0.42 ± 0.14	1.2 ± 0.4	7.9 ± 1.9
Akita	-	14.7 ± 1.2****	0.31 ± 0.03**	1.3 ± 0.3	7.3 ± 2.0
	+	15.8 ± 1.4****	0.29 ± 0.03**	1.2 ± 0.5	7.8 ± 1.5
STZ	-	19.7 ± 4.3****	0.27 ± 0.07**	1.1 ± 0.5	7.0 ± 1.5
	+	19.1 ± 3.5****	0.28 ± 0.05**	1.3 ± 0.6	7.5 ± 1.3

*n* = 5–8/group.

\*\**P* < 0.01 and \*\*\*\**P* < 0.0001 compared to ApoE<sup>-/-</sup> controls.

quantified in the central, mid-, and peripheral retinal regions. All morphometric analyses were performed while blinded to treatment group.

### Cryosectioning

Mouse eyes were fixed in 30% (w/v) sucrose at 4°C overnight and then with increasing concentrations of Tissue-Tek optimal cutting temperature (OCT) compound (Sakura Finetek USA, Torrance, California). These fixation steps aid in maintaining the morphology of the retinal sections and in preventing ice crystal formation during flash freezing. The eyes were then embedded in OCT and flash frozen with liquid nitrogen. Samples were stored at -80°C.

Frozen eyes embedded in OCT blocks were cryosectioned along the frontal/coronal plane at -20°C at a thickness of 10 μm. Sections were then frozen at -20°C until use for immunostaining and retinal thickness measurements (refer to Supplementary Figure S1).

### Immunofluorescent Staining

Immunofluorescent staining was performed on cryosections. Slides were incubated in 4% paraformaldehyde at room temperature for 30 minutes. After blocking with 10% normal serum for 1 hour, sections were incubated with primary antibodies against 78-kDa glucose-regulated protein (GRP78) and C/EBP homologous protein (CHOP), also known as growth arrest- and DNA damage-inducible gene 153 (GADD153) (Santa Cruz, Dallas, TX, USA), at 4°C overnight and 1:100 dilution. The following day, sections were incubated in Alexa Fluor 488-conjugated secondary antibodies (Thermo Fisher, Waltham, MA, USA) for 1.5 hours at 1:250 dilution. Images of the stained sections were acquired using an Olympus BX41 microscope connected to an Olympus DP71 camera. Immunofluorescent staining intensity was quantified and normalized to retinal area using ImageJ (v1.48; National Institutes of Health, Bethesda, MD, USA) software. The first third of the frontal cross sections, taken from the front/corneal side of the eye, corresponds to the peripheral retinal region, the next third corresponds to the midretinal region, and the final third taken nearest to the optic nerve corresponds to the central retinal region.

### Statistical Analysis

Data are reported as mean ± SD. Two-way ANOVA with Bonferroni's multiple comparison test was performed using GraphPad Prism (v6.01; GraphPad Software, La Jolla, CA,

USA) to assess differences between treatment groups. Probability values of *P* < 0.05 were considered to indicate statistical significance.

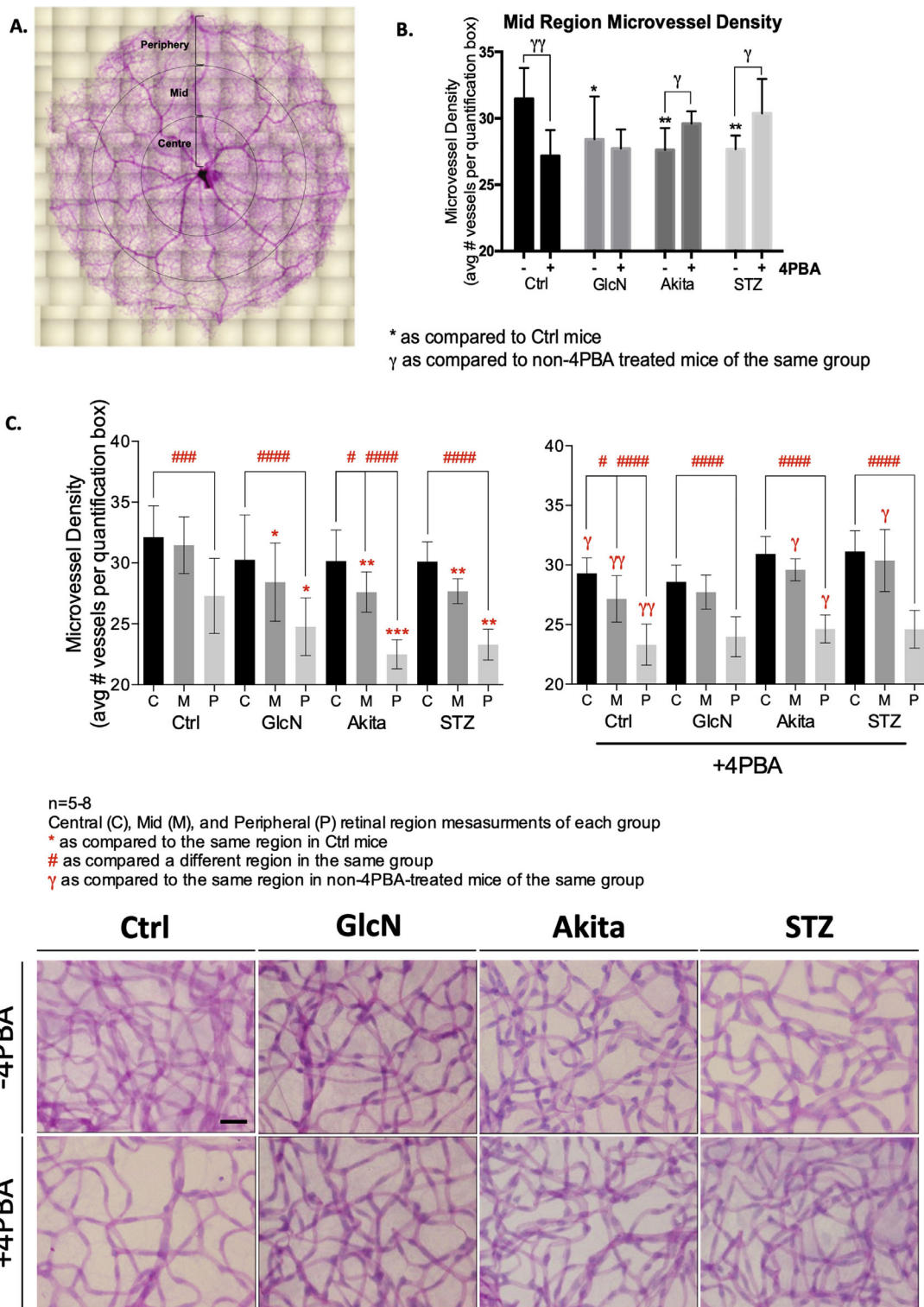
## RESULTS

### STZ Injections and the Ins2<sup>+Akita</sup> Point Mutation Induce Hyperglycemia and Insulinopenia in ApoE<sup>-/-</sup> Mice Without Altering Lipid Levels

In accordance with previous work,<sup>42,43</sup> our results demonstrate that both STZ injections and the Ins2<sup>+Akita</sup> point mutation promote insulinopenia and hyperglycemia (Table). STZ injections and the Ins2<sup>+Akita</sup> point mutation induced a 2.4-fold and 1.8-fold increase in fasting blood glucose, relative to ApoE<sup>-/-</sup> controls, and fasting plasma insulin levels of these groups were significantly lower than controls. Plasma triglyceride and cholesterol levels were not significantly different between groups at 15 weeks of age (Table). GlcN-supplemented mice had similar plasma insulin, glucose, triglyceride, and cholesterol levels compared to control mice.<sup>34,35</sup> 4PBA treatment did not alter fasting blood glucose, plasma insulin, or lipid levels in any of the four subsets of mice (Table). Together, these data indicate that the mouse models used in this study can be used to investigate the progression of diabetic complications attributed to increased blood glucose levels or glucose metabolite levels (i.e., glucosamine), independent of changes in plasma lipid levels.

### Hyperglycemia Reduces Microvessel Density in Mid- and Peripheral Retinal Regions

The regions considered for all morphometric analyses on the retinal trypsin digests are highlighted in Figure 1A. All experimental groups presented with an overall reduction in retinal microvessel density from the optic disk (where the density is greatest) to the peripheral retina (where the density is lowest). GlcN-supplemented ApoE<sup>-/-</sup>, STZ-injected ApoE<sup>-/-</sup>, and ApoE<sup>-/-</sup>:Ins2<sup>+Akita</sup> mice presented with significantly lower microvessel density in the mid- and peripheral retinal regions relative to control mice (Figs. 1B, 1C). Although there was a trend toward decreased microvessel density in the central regions of GlcN-supplemented ApoE<sup>-/-</sup>, STZ-injected ApoE<sup>-/-</sup>, and ApoE<sup>-/-</sup>:Ins2<sup>+Akita</sup> mice compared to controls, this did not reach statistical significance. 4PBA treatment rescued the decline in microvessel density in the mid- and peripheral regions of STZ-injected ApoE<sup>-/-</sup> and ApoE<sup>-/-</sup>:Ins2<sup>+Akita</sup>



\* as compared to Ctrl mice  
 $\gamma$  as compared to non-4PBA treated mice of the same group

n=5-8  
 Central (C), Mid (M), and Peripheral (P) retinal region measurements of each group  
 \* as compared to the same region in Ctrl mice  
 # as compared a different region in the same group  
 $\gamma$  as compared to the same region in non-4PBA-treated mice of the same group

**FIGURE 1.** Retinal microvascular density. **(A)** Representative image of a retinal flatmount prepared by trypsin digestion and PAS staining. The central retinal region is defined as the circular region closest to the optic disc, while the periphery is the outer ring. **(B)** Microvessel density in the midretina showing the effects of 4PBA.  $n = 5-8$ . **(C)** Microvessel density was quantified in each treatment group in the central (C), mid (M), and peripheral (P) retina. \* $P < 0.05$ , \*\* $P < 0.005$ , and \*\*\* $P < 0.0005$  as compared to the same region in control mice. # $P < 0.05$ , ## $P < 0.005$ , ### $P < 0.0005$ , and #### $P < 0.00005$  as compared to a different region within the same group.  $\gamma P < 0.05$  and  $\gamma\gamma P < 0.005$  as compared to non-4PBA-treated mice of the same group. Refer to legend below graph. **(D)** Representative images of 4PBA and non-4PBA-treated groups showing average microvessel density. Scale bar: 50  $\mu$ m.

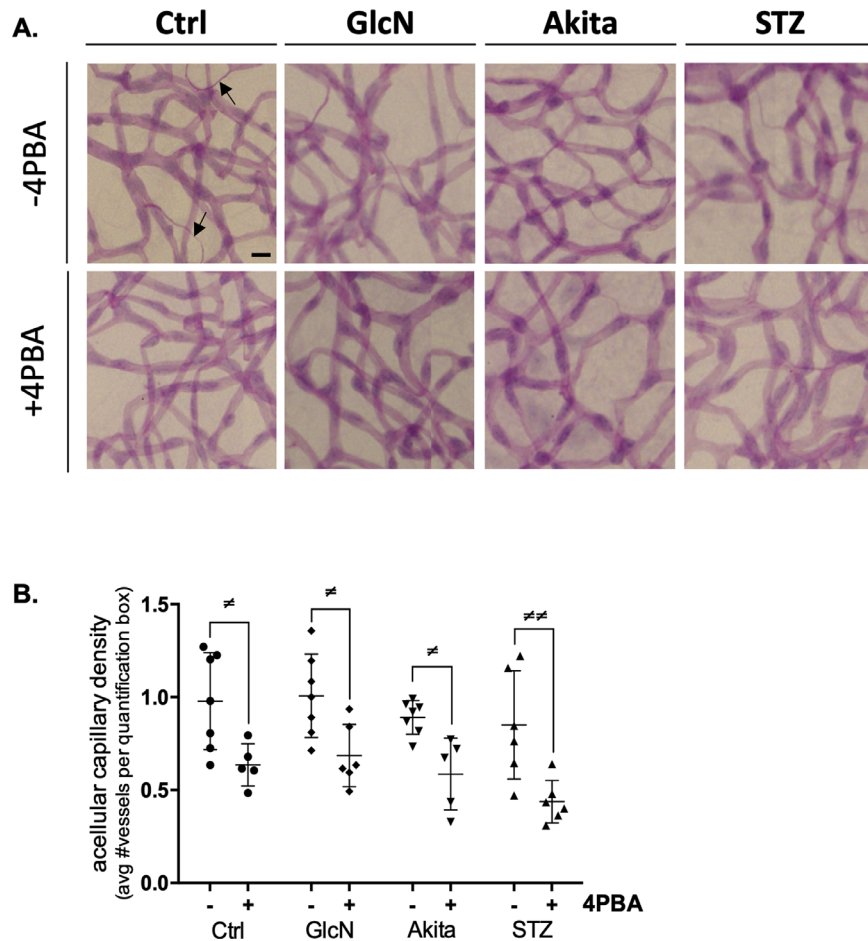


**FIGURE 2.** Acellular capillaries. (A) Representative images of acellular capillaries in 4PBA and non-4PBA-treated sections from each group. Examples of acellular capillaries are indicated by *black arrows*. Scale bar: 10  $\mu$ m. (B) Acellular capillaries were quantified in the midregion of the retina.  $n = 5-7$ . \* $P < 0.05$  and \*\* $P < 0.005$  as compared to non-4PBA-treated mice of the same group.

mice (Figs. 1B, 1C, 1D). Interestingly, 4PBA significantly reduced retinal microvessel density in the control mice (Figs. 1B, 1D).

### Acellular Capillary Density Is Significantly Reduced With 4PBA Supplementation

Acellular capillary density was quantified in the midretinal region. Between-group analyses revealed a significant reduction in acellular capillary density in 4PBA-treated mice relative to non-4PBA-treated mice of the same experimental group (Fig. 2). However, there was no significant difference in acellular capillary density between controls and experimental groups.

### 4PBA Supplementation Rescues Increased Pericyte Ghost Density in Mice With High Blood Glucose or Glucosamine Levels

Pericyte ghost density in the peripheral retina of GlcN-supplemented ApoE<sup>-/-</sup>, STZ-injected ApoE<sup>-/-</sup>, and ApoE<sup>-/-</sup>:Ins2<sup>+Akita</sup> mice was significantly increased relative to control mice (Fig. 3). There was a trend toward increased

pericyte ghost density in the central and midregions of GlcN-supplemented ApoE<sup>-/-</sup> and ApoE<sup>-/-</sup>:Ins2<sup>+Akita</sup> groups relative to control mice, but this did not reach statistical significance. Only STZ-injected mice had significantly increased pericyte ghost densities in all three retinal regions compared to control mice. 4PBA treatment reduced pericyte ghost density in all three retinal regions in GlcN-supplemented, STZ-injected, and ApoE<sup>-/-</sup>:Ins2<sup>+Akita</sup> mice, but the difference was most pronounced in the retinal periphery. In control mice, although there was a trend toward reduced pericyte ghosts with 4PBA treatment, the differences did not reach statistical significance.

### Some ER Stress Markers Are Upregulated Under Hyperglycemic Conditions

Overall retinal GRP78 levels were similar between all groups and were unchanged by 4PBA treatment (Figs. 4A, 4B). GRP78 expression in only in the midretinal region of ApoE<sup>-/-</sup>:Ins2<sup>+Akita</sup> mice was significantly increased relative to control mice. Additionally, 4PBA treatment increased GRP78 expression in the midretina of the control mice. However, no significant alterations in GRP78 expression

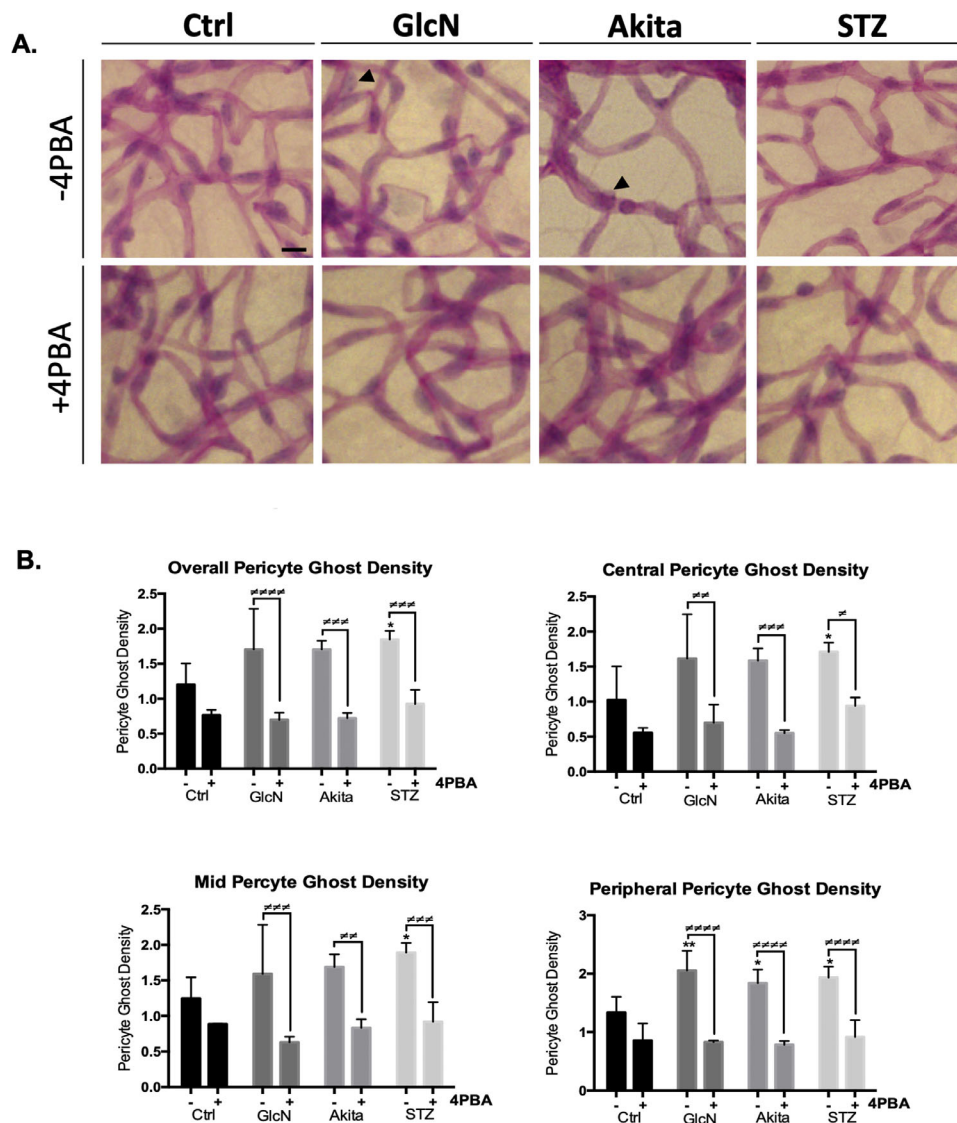


**FIGURE 3.** Pericyte ghosts. (A) Representative images of pericyte ghosts in 4PBA and non-4PBA-treated sections from each group. Examples of pericyte ghosts are indicated by *black arrowheads*. Scale bar: 10  $\mu$ m. (B) Pericyte ghosts were quantified in the central, mid-, and peripheral retina. Data are presented as the average number of pericyte ghosts per quantification box.  $n = 3-4$ . \* $P < 0.05$  and \*\* $P < 0.005$  as compared to the same region in control mice. # $P < 0.05$ , ## $P < 0.005$ , ### $P < 0.0005$ , and #### $P < 0.00005$  as compared to the same region in non-4PBA-treated mice of the same group.

in the central and peripheral retina were observed in any group.

Between-group analyses revealed that CHOP expression in the mid- and peripheral retina of ApoE<sup>-/-</sup>:Ins2<sup>+/Akita</sup> was significantly increased relative to control mice (Figs. 4C, 4D). There was a trend toward increased CHOP expression in the mid- and peripheral retina of GlcN-supplemented ApoE<sup>-/-</sup> and STZ-injected ApoE<sup>-/-</sup> mice compared to control mice, but this did not reach statistical significance. 4PBA decreased CHOP expression in the peripheral retina of GlcN-supplemented ApoE<sup>-/-</sup>, STZ-injected ApoE<sup>-/-</sup>, and ApoE<sup>-/-</sup>:Ins2<sup>+/Akita</sup> mice relative to their untreated counterparts. 4PBA also reduced overall CHOP levels in control mice.

## DISCUSSION

To our knowledge, this is the first study to analyze the effects of an ER stress inhibitor (4PBA) on the progression of DR symptoms in four different mouse models. This study focused on the assessment of three major morphologic hallmarks of DR: reduced microvessel density, increased acellular capillaries, and increased pericyte ghosts. We also performed a preliminary examination of ER stress-related protein expression. ER stress has been identified as a causal factor for atherosclerotic development in ApoE<sup>-/-</sup> mice.<sup>44-46</sup> Increased levels of ER stress have been observed in chemical (STZ-injected ApoE<sup>-/-</sup>) and genetic (ApoE<sup>-/-</sup>:Ins2<sup>+/Akita</sup>) mouse models of hyperglycemia.<sup>47</sup> Glucosamine, which is

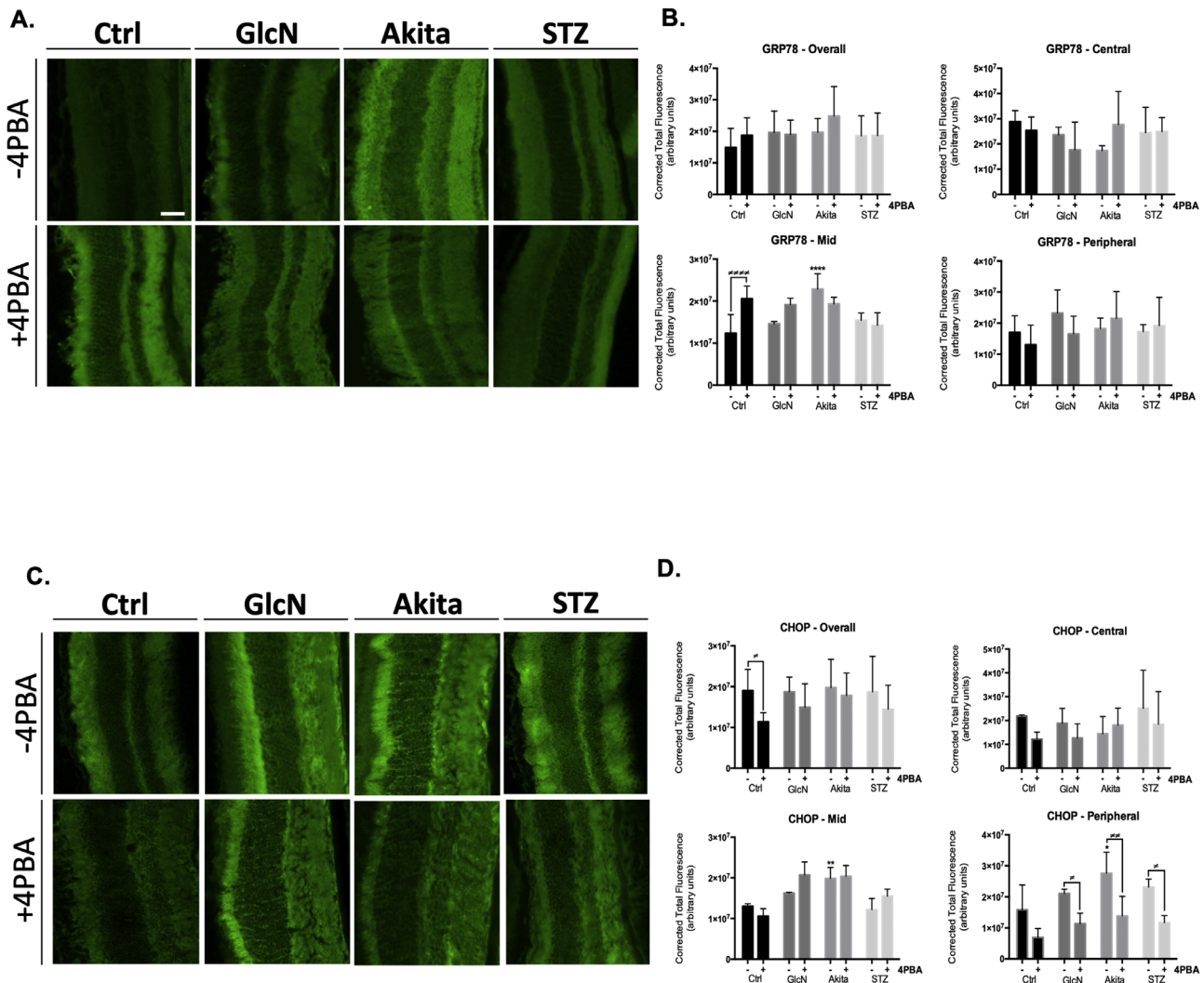


**FIGURE 4.** GRP78 and CHOP expression in retinas. Representative images of cryostat sectioned retinas from 15-week-old mice immunostained for GRP78 (A) and CHOP (C). Scale bar: 50  $\mu$ m. Fluorescence intensity of GRP78 (B) and CHOP (D) was measured using ImageJ software and normalized to account for changes in area.  $n = 3-6$ . \* $P < 0.05$  and \*\* $P < 0.005$  as compared to the same region in control mice.  $\#P < 0.05$  and  $\#\#P < 0.005$  as compared to the same region in non-4PBA-treated mice of the same group.

a product of glucose flux through the hexosamine pathway and an ER stress-inducing agent, has been linked to diabetic atherogenesis.<sup>35,48</sup> The inclusion of the GlcN-supplemented treatment group allowed for comparison of the effects of ER stress alone under normoglycemic conditions.

The decline in microvessel density from the optic disc to the peripheral retina seen across all groups, including control mice, is consistent with observations made in the healthy human retina.<sup>49</sup> However, it is uncertain if the decrease seen in ApoE<sup>-/-</sup> mice is representative of healthy mice or if it is exacerbated by the ApoE<sup>-/-</sup> genotype. Interestingly, hyperglycemic mice showed no difference in acellular capillary density compared to control mice. This is inconsistent with the findings from previous studies in which STZ-injected mice and ApoE<sup>-/-</sup>:Ins2<sup>+/Akita</sup> mice were observed to have significantly increased acellular capillary densities relative to wild-type controls.<sup>42,50,51</sup> Pericyte loss is believed to precede acellular capillary development, which may explain the presence of increased numbers of pericyte ghosts in the

experimental groups without an increase in acellular capillaries.<sup>10,52,53</sup> It is also possible that the similarity in acellular capillary density between control mice and treatment groups is a result of the pathophysiology (dyslipidemia) of the ApoE<sup>-/-</sup> control, which may contribute to increased acellular capillary development relative to wild-type (normolipidemic) controls used in other studies.<sup>42,50,54</sup> The protein kinase C pathway, which has been found to contribute to acellular capillary development, is upregulated in ApoE<sup>-/-</sup> mice and could cause an increase in acellular capillaries in ApoE<sup>-/-</sup> mice to the level of the experimental groups.<sup>55-57</sup> The ability of 4PBA to reduce acellular capillary density is consistent with previous studies.<sup>19,58</sup>

Differences in pericyte ghost densities between controls and experimental groups, as well as between 4PBA and non-4PBA-treated mice within the same group, increased in significance moving outward from the optic disc. The trends observed with respect to pericyte ghost and microvessel vessel density in GlcN-supplemented mice are very similar to those in STZ-injected and ApoE<sup>-/-</sup>:Ins2<sup>+/Akita</sup> mice,

suggesting that ER stress, even in the absence of hyperglycemia, may be a contributor to DR pathogenesis.<sup>19,29,59,60</sup>

The UPR is an adaptive signal transduction pathway to maintain ER homeostasis.<sup>61</sup> The UPR is activated by three ER stress sensors: inositol requiring enzyme 1 $\alpha$ , PKR-like ER kinase (PERK), and activating transcription factor 6 $\alpha$ .<sup>62</sup> Under homeostatic conditions, these ER stress sensors remain inactivated through association with a chaperone called binding immunoglobulin protein (BiP), also known as GRP78.<sup>62</sup> However, as misfolded proteins accumulate in the ER, BiP dissociates from the UPR sensors and binds to the hydrophobic domains of the misfolded proteins with a greater affinity, allowing for activation of downstream signaling pathways by the UPR sensors.<sup>63–65</sup> The adaptive UPR functions to restore homeostasis and mitigate ER stress, but when this fails, a proapoptotic response is initiated.<sup>66</sup> Under chronic ER stress, PERK upregulates the transcription of GADD153/CHOP, which inhibits the expression of the anti-apoptotic (BCL-2) to induce cell death.<sup>67,68</sup> Levels of GRP78 (adaptive UPR) and CHOP (apoptotic UPR) were measured in the retinas of mice in each of the experimental groups. These markers indicate the initiation of two key steps in the ER stress pathway.

Li et al.<sup>19</sup> have noted increased GRP78 expression in the retinas of ApoE<sup>-/-</sup>:Ins2<sup>+Akita</sup> mice, relative to controls. This is consistent with observation of increased GRP78 expression in the midretinal region in this study. 4PBA did not have any significant effect on GRP78 expression, except for the increase seen in control mice in the midregion. This, taken with the microvessel data showing that 4PBA further increased microvessel density in control mice, suggests that 4PBA may have a toxic effect in ApoE<sup>-/-</sup> mice. 4PBA is a histone deacetylase inhibitor that has been shown to induce the expression of certain ER chaperones, including GRP78.<sup>60,69,70</sup> The extent of GRP78 induction has been found to be positively correlated with the amount of histone acetylation.<sup>69</sup> Previous reports have shown that 4PBA increases GRP78 expression in control groups of some cell types.<sup>71,72</sup>

CHOP expression was increased in ApoE<sup>-/-</sup>:Ins2<sup>+Akita</sup> mice relative to controls in the mid- and peripheral retina, which is consistent with the literature.<sup>73</sup> There was a trend toward increased CHOP expression in STZ-injected and GlcN-treated mice. 4PBA reduced CHOP expression in the peripheral retina but not in other regions of the experimental groups. This suggests that there are regional differences in the response to hyperglycemic conditions, including a heightened ER stress response further outward from the optic disc, as well as increased susceptibility to ER stress-inhibiting agents. There are multiple mechanisms that may account for the diverse effects of 4PBA in various retinal regions and treatment groups. 4PBA is a nonspecific chemical chaperone and a histone deacetylase inhibitor.<sup>73,74</sup> 4PBA has a variety of uses, including as a treatment for urea cycle disorders because of its ability to act as a nitrogen sink.<sup>75</sup> Additional applications of 4PBA are currently being studied in areas including cancer, hemoglobinopathies, cystic fibrosis, and motor neuron diseases.<sup>74</sup> In relation to diabetes, 4PBA has been found to improve diabetic encephalopathy and nephropathy, muscle atrophy, inflammation, and  $\beta$ -cell apoptosis.<sup>58,76–81</sup> The reduction in CHOP expression with 4PBA suggests that 4PBA effectively alleviates ER stress to suppress the proapoptotic UPR.<sup>68,82</sup>

Overall, this work characterizes the pathologic changes associated with DR in three different mouse models of diabetic atherosclerosis. The results show that

hyperglycemia is sufficient to promote DR. Furthermore, a downstream metabolite of glucose (glucosamine) can promote DR in the absence of changes in glucose and insulin levels. Finally, the findings from this study support a role for ER stress in the development of DR and suggest that alleviation of ER stress can protect against DR progression.

### Acknowledgments

Supported by the Heart and Stroke Foundation of Canada (HSFC) (G-17-0017029). GHW is supported by a HSFC Ontario Mid-Career Investigator Award.

Disclosure: **V. Mazzoli**, None; **L.H. Zhong**, None; **V.T. Dang**, None; **Y. Shi**, None; **G.H. Werstuck**, None

### References

- Hendrick AM, Gibson M-V, Kulshreshtha A. Diabetic retinopathy. *Prim Care*. 2015;42:451–464.
- Alberti KGMM, Zimmet PZ. Definition, diagnosis and classification of diabetes mellitus and its complications. Part 1: Diagnosis and classification of diabetes mellitus. Provisional report of a WHO consultation. *Diabet Med*. 1998;15:539–553.
- Nathan DM, Zinman B, Cleary PA, et al. Modern-day clinical course of type 1 diabetes mellitus after 30 years' duration: the Diabetes Control and Complications Trial Diabetes Control and Complications Trial/Epidemiology of Diabetes Interventions and Complications (DCCT/EDIC) study research group. *Arch Intern Med*. 2009;169:1307–1316.
- Kong D-Q, Li L, Liu Y, Zheng G-Y. Association between endoplasmic reticulum stress and risk factors of diabetic retinopathy. *Int J Ophthalmol*. 2018;11:1704–1710.
- Zhang SX, Ma JH, Bhatta M, Fliesler SJ, Wang JJ. The unfolded protein response in retinal vascular diseases: implications and therapeutic potential beyond protein folding. *Prog Retin Eye Res*. 2015;45:111–131.
- Gariano RF, Gardner TW. Retinal angiogenesis in development and disease. *Nature*. 2005;438:960–966.
- Zhang SX, Ma J-X. Ocular neovascularization: implication of endogenous angiogenic inhibitors and potential therapy. *Prog Retin Eye Res*. 2007;26:1–37.
- Mizutani M, Kern TS, Lorenzi M. Accelerated death of retinal microvascular cells in human and experimental diabetic retinopathy. *J Clin Invest*. 1996;97:2883–2890.
- Kern TS, Engerman RL. Comparison of retinal lesions in alloxan-diabetic rats and galactose-fed rats. *Curr Eye Res*. 1994;13:863–867.
- Hammes HP, Feng Y, Pfister F, Brownlee M. Diabetic retinopathy: targeting vasoregression. *Diabetes*. 2011;60:9–16.
- Adamis AP, Miller JW, Bernal MT, et al. Increased vascular endothelial growth factor levels in the vitreous of eyes with proliferative diabetic retinopathy. *Am J Ophthalmol*. 1994;118:445–450.
- Aiello LP, Arrigg PG, Shah ST, et al. Vascular endothelial growth factor in ocular fluid of patients with diabetic retinopathy and other retinal disorders. *N Engl J Med*. 1994;331:1480–1487.
- Kroeger H, Chiang WC, Felden J, Nguyen A, Lin JH. ER stress and unfolded protein response in ocular health and disease. *FEBS J*. 2019;286:399–412.
- Engerman RL, Kern TS. Retinopathy in animal models of diabetes. *Diabetes Metab Rev*. 1995;11:109–120.

15. Antonetti DA, Lieth E, Barber AJ, Gardner TW. Molecular mechanisms of vascular permeability in diabetic retinopathy. *Semin Ophthalmol*. 1999;14:240–248.
16. Antonetti DA, Barber AJ, Bronson SK, et al. Diabetic retinopathy: seeing beyond glucose-induced microvascular disease. *Diabetes*. 2006;55:2401–2411.
17. Yang J, Chen C, McLaughlin T, et al. Loss of X-box binding protein 1 in Müller cells augments retinal inflammation in a mouse model of diabetes. *Diabetologia*. 2019;62:531–543.
18. Li J, Wang JJ, Zhang SX. Preconditioning with endoplasmic reticulum stress mitigates retinal endothelial inflammation via activation of X-box binding protein 1. *J Biol Chem*. 2011;286:4912–4921.
19. Li J, Wang JJ, Yu Q, Wang M, Zhang SX. Endoplasmic reticulum stress is implicated in retinal inflammation and diabetic retinopathy. *FEBS Lett*. 2009;583:1521–1527.
20. Jing G, Wang JJ, Zhang SX. ER stress and apoptosis: a new mechanism for retinal cell death. *Exp Diabetes Res*. 2012;2012:589589.
21. Zhang SX, Sanders E, Fliesler SJ, Wang JJ. Endoplasmic reticulum stress and the unfolded protein responses in retinal degeneration. *Exp Eye Res*. 2014;125:30–40.
22. El-Remessy AB, Rajesh M, Mukhopadhyay P, et al. Cannabinoid 1 receptor activation contributes to vascular inflammation and cell death in a mouse model of diabetic retinopathy and a human retinal cell line. *Diabetologia*. 2011;54:1567–1578.
23. Gu X, El-Remessy AB, Brooks SE, Al-Shabrawey M, Tsai NT, Caldwell RB. Hyperoxia induces retinal vascular endothelial cell apoptosis through formation of peroxynitrite. *Am J Physiol Cell Physiol*. 2003;285:C546–C554.
24. Busik JV, Mohr S, Grant MB. Hyperglycemia-induced reactive oxygen species toxicity to endothelial cells is dependent on paracrine mediators. *Diabetes*. 2008;57:1952–1965.
25. Li H, Zhu X, Fang F, Jiang D, Tang L. Down-regulation of GRP78 enhances apoptosis via CHOP pathway in retinal ischemia-reperfusion injury. *Neurosci Lett*. 2014;575:68–73.
26. Tajiri S, Oyadomari S, Yano S, et al. Ischemia-induced neuronal cell death is mediated by the endoplasmic reticulum stress pathway involving CHOP. *Cell Death Differ*. 2004;11:403–415.
27. Elmasry K, Ibrahim AS, Saleh H, et al. Role of endoplasmic reticulum stress in 12/15-lipoxygenase-induced retinal microvascular dysfunction in a mouse model of diabetic retinopathy. *Diabetologia*. 2018;61:1220–1232.
28. Oyadomari S, Mori M. Roles of CHOP/GADD153 in endoplasmic reticulum stress. *Cell Death Differ*. 2004;11:381–389.
29. Chen Y, Wang JJ, Li J, et al. Activating transcription factor 4 mediates hyperglycaemia-induced endothelial inflammation and retinal vascular leakage through activation of STAT3 in a mouse model of type 1 diabetes. *Diabetologia*. 2012;55:2533–2545.
30. Ballagh RA, Werstuck GH, Venegas-Pino D. Effects of hyperglycemia on endothelial activation and early atherosclerotic plaque development. *Atheroscler Suppl*. 2018;32:86–87.
31. Stoute H, Venegas-Pino D, Shi Y, Werstuck G. Hyperglycaemic apolipoprotein-E deficient mice have accelerated atherosclerosis and aberrant vasa vasorum neovascularization. *Can J Cardiol*. 2014;30:S269–S270.
32. Venegas-Pino DE, Lagrotteria A, Wang PW, et al. Evidence of extensive atherosclerosis, coronary artery disease and myocardial infarction in the ApoE<sup>-/-</sup>:Ins2<sup>+Akita</sup> mouse fed a Western diet. *Atherosclerosis*. 2018;275:88–96.
33. Dang VT, Zhong LH, Huang A, Deng A, Werstuck GH. Glycosphingolipids promote pro-atherogenic pathways in the pathogenesis of hyperglycemia-induced accelerated atherosclerosis. *Metabolomics*. 2018;14:92.
34. Huang A, Young TL, Dang VT, Shi Y, McAlpine CS, Werstuck GH. 4-Phenylbutyrate and valproate treatment attenuates the progression of atherosclerosis and stabilizes existing plaques. *Atherosclerosis*. 2017;266:103–112.
35. Werstuck GH, Khan MI, Femia G, et al. Glucosamine-induced endoplasmic reticulum dysfunction is associated with accelerated atherosclerosis in a hyperglycemic mouse model. *Diabetes*. 2006;55:93–101.
36. Beriault DR, Sharma S, Shi Y, Khan MI, Werstuck GH. Glucosamine-supplementation promotes endoplasmic reticulum stress, hepatic steatosis and accelerated atherogenesis in apoE<sup>-/-</sup> mice. *Atherosclerosis*. 2011;219:134–140.
37. Venegas-Pino DE, Wang PW, Stoute HK, et al. Sex-specific differences in an ApoE<sup>-/-</sup>:Ins2<sup>+Akita</sup> mouse model of accelerated atherosclerosis. *Am J Pathol*. 2016;186:67–77.
38. Chou JC, Rollins SD, Fawzi AA. Trypsin digest protocol to analyze the retinal vasculature of a mouse model. *J Vis Exp*. 2013;76:e50489.
39. Dietrich N, Hammes H-P. Retinal digest preparation: a method to study diabetic retinopathy. In: Joost HG, Al-Hasani H, Schürmann A, eds. *Animal Models in Diabetes Research. Methods in Molecular Biology (Methods and Protocols)*. Totowa, NJ: Humana Press; 2012;933:291–302.
40. Browning J, Wylie CK, Gole G. Quantification of oxygen-induced retinopathy in the mouse. *Invest Ophthalmol Vis Sci*. 1997;38:1168–1174.
41. Kern TS, Tang J, Mizutani M, et al. Response of capillary cell death to aminoguanidine predicts the development of retinopathy: comparison of diabetes and galactosemia. *Invest Ophthalmol Vis Sci*. 2000;41:3972–3978.
42. Barber AJ, Antonetti DA, Kern TS, et al. The Ins2Akita mouse as a model of early retinal complications in diabetes. *Invest Ophthalmol Vis Sci*. 2005;46:2210–2218.
43. Like AA, Rossini AA. Streptozotocin-induced pancreatic insulinitis: new model of diabetes mellitus. *Science*. 1976;193:415–417.
44. Véniant MM, Withycombe S, Young SG. Lipoprotein size and atherosclerosis susceptibility in ApoE<sup>-/-</sup> and Ldlr<sup>-/-</sup> mice. *Arterioscler Thromb Vasc Biol*. 2001;21:1567–1570.
45. Zhou L, Yang D, Wu DF, Guo ZM, Okoro E, Yang H. Inhibition of endoplasmic reticulum stress and atherosclerosis by 2-aminopurine in apolipoprotein E-deficient mice. *ISRN Pharmacol*. 2013;2013:847310.
46. Geng J, Xu H, Fu W, et al. Rosuvastatin protects against endothelial cell apoptosis in vitro and alleviates atherosclerosis in ApoE<sup>-/-</sup> mice by suppressing endoplasmic reticulum stress. *Exp Ther Med*. 2020;20:550.
47. King AJF. The use of animal models in diabetes research. *Br J Pharmacol*. 2012;166:877–894.
48. Kim AJ, Shi Y, Austin RC, Werstuck GH. Valproate protects cells from ER stress-induced lipid accumulation and apoptosis by inhibiting glycogen synthase kinase-3. *J Cell Sci*. 2005;118:89–99.
49. Campbell JP, Zhang M, Hwang TS, et al. Detailed vascular anatomy of the human retina by projection-resolved optical coherence tomography angiography. *Sci Rep*. 2017;7:42201.
50. Weerasekera LY, Balmer LA, Ram R, Morahan G. Characterization of retinal vascular and neural damage in a novel model of diabetic retinopathy. *Invest Ophthalmol Vis Sci*. 2015;56:3721–3730.
51. Bhatta M, Chatpar K, Hu Z, Wang JJ, Zhang SX. Reduction of endoplasmic reticulum stress improves angiogenic progenitor cell function in a mouse model of type 1 diabetes. *Cell Death Dis*. 2018;9:1–14.
52. Li C, Wang L, Huang K, Zheng L. Endoplasmic reticulum stress in retinal vascular degeneration: protective role of resveratrol. *Invest Ophthalmol Vis Sci*. 2012;53:3241–3249.

53. Hammes H, Lin J, Wagner P, et al. Angiopoietin-2 causes pericyte dropout in the normal retina. *Diabetes*. 2004;53:1104–1110.
54. Valdez CN, Arboleda-Velasquez JF, Amarnani DS, Kim LA, D'Amore PA. Retinal microangiopathy in a mouse model of inducible mural cell loss. *Am J Pathol*. 2014;184:2618–2626.
55. Rask-Madsen C, King GL. Vascular complications of diabetes: mechanisms of injury and protective factors. *Cell Metab*. 2013;17:20–33.
56. Gupta A, Bhatnagar S. Vasoregression: a shared vascular pathology underlying macrovascular and microvascular pathologies? *Omi A J Integr Biol*. 2015;19:733–753.
57. Harja E, Jong SC, Lu Y, et al. Mice deficient in PKC $\beta$  and apolipoprotein E display decreased atherosclerosis. *FASEB J*. 2009;23:1081–1091.
58. Shruthi K, Reddy SS, Chitra PS, Reddy GB. Ubiquitin-proteasome system and ER stress in the brain of diabetic rats. *J Cell Biochem*. 2019;120:5962–5973.
59. Adachi T, Yasuda H, Nakamura S, et al. Endoplasmic reticulum stress induces retinal endothelial permeability of extracellular-superoxide dismutase. *Free Radic Res*. 2011;45:1083–1092.
60. Ghodke-Puranik Y, Thorn CF, Lamba JK, et al. Valproic acid pathway: pharmacokinetics and pharmacodynamics. *Pharmacogenet Genomics*. 2013;23:236–241.
61. Hetz C, Chevet E, Oakes SA. Proteostasis control by the unfolded protein response. *Nat Cell Biol*. 2015;17:829–838.
62. Grootjans J, Kaser A, Kaufman RJ, Blumberg RS. The unfolded protein response in immunity and inflammation. *Nat Rev Immunol*. 2016;16:469.
63. Shen J, Chen X, Hendershot L, Prywes R. ER stress regulation of ATF6 localization by dissociation of BiP/GRP78 binding and unmasking of Golgi localization signals. *Dev Cell*. 2002;3:99–111.
64. Bertolotti A, Zhang Y, Hendershot LM, Harding HP, Ron D. Dynamic interaction of BiP and ER stress transducers in the unfolded-protein response. *Nat Cell Biol*. 2000;2:326–332.
65. Pincus D, Chevalier MW, Aragón T, et al. BiP binding to the ER-stress sensor Ire1 tunes the homeostatic behavior of the unfolded protein response. *PLoS Biol*. 2010;8:e1000415.
66. Hetz C. The unfolded protein response: controlling cell fate decisions under ER stress and beyond. *Nat Rev Mol Cell Biol*. 2012;13:89–102.
67. McCullough KD, Martindale JL, Klotz L-O, Aw T-Y, Holbrook NJ. Gadd153 sensitizes cells to endoplasmic reticulum stress by down-regulating Bcl2 and perturbing the cellular redox state. *Mol Cell Biol*. 2001;21:1249–1259.
68. Marciniak SJ, Yun CY, Oyadomari S, et al. CHOP induces death by promoting protein synthesis and oxidation in the stressed endoplasmic reticulum. *Genes Dev*. 2004;18:3066–3077.
69. Shi Y, Gerritsma D, Bowes AJ, Capretta A, Werstuck GH. Induction of GRP78 by valproic acid is dependent upon histone deacetylase inhibition. *Bioorganic Med Chem Lett*. 2007;17:4491–4494.
70. Zhang ZZ, Tong NT, Gong YY, et al. Valproate protects the retina from endoplasmic reticulum stress-induced apoptosis after ischemia-reperfusion injury. *Neurosci Lett*. 2011;504:88–92.
71. Jiang X, Fang G, Dong L, et al. Chemical chaperone 4-phenylbutyric acid alleviates the aggregation of human familial pulmonary fibrosis-related mutant SP-A2 protein in part through effects on GRP78. *Biochim Biophys Acta Mol Basis Dis*. 2018;1864:3546–3557.
72. Reddy SS, Shruthi K, Joy D, Reddy GB. 4-PBA prevents diabetic muscle atrophy in rats by modulating ER stress response and ubiquitin-proteasome system. *Chem Biol Interact*. 2019;306:70–77.
73. Ma JH, Wang JJ, Zhang SX. The unfolded protein response and diabetic retinopathy. *J Diabetes Res*. 2014;2014:160140.
74. Petri S, Kiaei M, Kipiani K, et al. Additive neuroprotective effects of a histone deacetylase inhibitor and a catalytic antioxidant in a transgenic mouse model of amyotrophic lateral sclerosis. *Neurobiol Dis*. 2006;22:40–49.
75. Erbay E, Babaev VR, Mayers JR, et al. Reducing endoplasmic reticulum stress through a macrophage lipid chaperone alleviates atherosclerosis. *Nat Med*. 2009;15:1383–1391.
76. Iannitti T, Palmieri B. Clinical and experimental applications of sodium phenylbutyrate. *Drugs R D*. 2011;11:227–249.
77. Reddy SS, Shruthi K, Joy D, Reddy GB. 4-PBA prevents diabetic muscle atrophy in rats by modulating ER stress response and ubiquitin-proteasome system. *Chem Biol Interact*. 2019;306:70–77.
78. Kawasaki N, Asada R, Saito A, Kanemoto S, Imaizumi K. Obesity-induced endoplasmic reticulum stress causes chronic inflammation in adipose tissue. *Sci Rep*. 2012;2:799.
79. Wang Z, Huang Y, Cheng Y, et al. Endoplasmic reticulum stress-induced neuronal inflammatory response and apoptosis likely plays a key role in the development of diabetic encephalopathy. *Oncotarget*. 2016;7:78455–78472.
80. Qi W, Mu J, Luo ZF, et al. Attenuation of diabetic nephropathy in diabetes rats induced by streptozotocin by regulating the endoplasmic reticulum stress inflammatory response. *Metabolism*. 2011;60:594–603.
81. Zhu M, Guo M, Fei L, Pan XQ, Liu QQ. 4-Phenylbutyric acid attenuates endoplasmic reticulum stress-mediated pancreatic  $\beta$ -cell apoptosis in rats with streptozotocin-induced diabetes. *Endocrine*. 2014;47:129–137.
82. Shore GC, Papa FR, Oakes SA. Signaling cell death from the endoplasmic reticulum stress response. *Curr Opin Cell Biol*. 2011;23:143–149.
83. Kim SJ, Yoo WS, Choi M, Chung I, Yoo JM, Choi WS. Increased O-GlcNAcylation of NF- $\kappa$ B enhances retinal ganglion cell death in streptozotocin-induced diabetic retinopathy. *Curr Eye Res*. 2016;41:249–257.
84. Lee VK, Hosking BM, Holeniewska J, et al. BTBR ob/ob mouse model of type 2 diabetes exhibits early loss of retinal function and retinal inflammation followed by late vascular changes. *Diabetologia*. 2018;61:2422–2432.